Mechanical Behavior of Blisters Spontaneously Formed by Multilayer 2D Materials

Wenxiang Wang, Xiaojie Ma, Zhaohe Dai, Shuai Zhang, Yuan Hou, Guorui Wang, Qunyang Li, Zhong Zhang,* Yueguang Wei,* and Luqi Liu*

Blisters can form spontaneously when transferring 2D materials on a substrate because of the small molecules trapped at the interface. Though extensive works have revealed a characteristic aspect ratio of these blisters by neglecting the bending effect of the layer, how the bending comes into play as the layer number increases has not been fully understood. Here, by simply measuring the profiles of blisters formed by transferred multilayer graphene and MoS_2 sheets, the variable profiles of blisters and the transition of their characteristic shape from a constant aspect ratio to a constant dome curvature are observed. Taking variable profiles of blisters and different characteristics of the interface into consideration, a theoretical model is established, and the mechanism of such transition is further analytically unveiled. In addition, based on this theory, the bending stiffness of sheets and the adhesion energy between sheets and substrates can be obtained simultaneously. This method is simple but robust, providing a new experimental way to explore the mechanical behavior of 2D material structures.

1. Introduction

In a range of biological and engineering systems, blisters form when a thin solid layer separates/delaminates from the substrate that it adheres to or is brought into contact with a substrate with some liquids or gases trapped at the layer–substrate interface.[1–3] Recently, blisters formed by atomically thin solids—2D materials—have spurred significant interest.[4,5]

Initially, 2D material blisters are considered as a nuisance in device applications as they are pockets of contaminants to obstruct contact between adjacent materials.[6] Recently, extensive efforts have been devoted to removing these 2D material blisters or fabricating 2D material devices with maximized clean areas.[7–13] More recently, however, interest in 2D material blisters themselves arises,[14] particularly because of the considerable strain and pressure associated with the deformation of the atomic layers that could be exploited in the tuning of the physical properties of the layer,[15–19] the development of high-pressure chemistry,[20,21] and the observation of nano-confined liquid molecules.[22]

Understanding the mechanics of 2D material blisters is very beneficial to many of these applications. A simple analytical model for how adhesion interacts with elasticity with both bending and stretching effect considered in gas-filled graphene blisters was first proposed by Yue et al.[23] In particular, when the stretching effect dominates over the bending effect, the aspect ratio (i.e., the height-to-radius ratio) of the blister is found to be a characteristic parameter that is controlled by the ratio of the layer–substrate adhesion to the in-plane stiffness of the layer.[23] However, the approximation

W. Wang, L. Liu
CAS Key Laboratory of Nanosystem and Hierarchical Fabrication
CAS Center for Excellence in Nanoscience
National Center for Nanoscience and Technology
Beijing 100190, China
E-mail: liulq@nanoctr.cn

W. Wang, L. Liu
University of Chinese Academy of Sciences
Beijing 100049, China

X. Ma, Y. Wei
Department of Mechanics and Engineering Science
College of Engineering
BIC-ESAT
Peking University
Beijing 100871, China
E-mail: weiyg@pku.edu.cn

Z. Dai
Mathematical Institute
University of Oxford
Woodstock Rd, Oxford OX2 6GG, UK

S. Zhang, Q. Li
Department of Engineering Mechanics and State Key Laboratory
of Tribology
Tsinghua University
Beijing 100084, China

Y. Hou, G. Wang, Z. Zhang
CAS Key Laboratory of Mechanical Behavior and Design of Materials
Department of Modern Mechanics
University of Science and Technology of China
Hefei 230027, China
E-mail: zhong.zhang@nanoctr.cn

of in-plane displacement fields in ref. [23] was later found not able to capture the radial strain accurately.[24] A recent work[25] has examined that largely improved accuracy could be achieved by Hencky's solution that has been widely used[26–28] as well as the analytical models by Dai et al.[29] The pioneering work by Khestanova et al. revealed the universal aspect ratio in a number of types of hydrocarbon/water-filled 2D material blisters (including graphene, hBN, and MoS$_2$) and further suggested their potential uses for the elasticity metrology of 2D materials and nanoscale confinements exerting on the trapped molecules.[30] Later, Sanchez et al. developed a simple analytical model to consider the surface tension of the trapped liquid contents and the slippage between the sheets and substrates.[31] With this, the characteristic aspect ratio of the blisters was exploited to extract the interfacial adhesion energy between layers and substrates.[31]

Though the characteristic aspect ratio (based on previous analysis that neglects the bending effect) has been widely observed in a variety of 2D material blisters,[25,30,31] its breakdown is expected when the bending of the thin sheet comes into play. Scaling analysis using a classical plate theory (in which bending stiffness is assumed to scale as Et^3 with E Young's modulus of the material and t the thickness of the layer) could suggest bending effect being important when the height of the blister is comparable to the thickness.[32] However, a detailed theoretical estimation is elusive since recent experiments have shown that 2D materials could exhibit much lower bending stiffness than what the classical plate theory assumed.[33,34]

Motived by the puzzle and opportunity associated with the bending behavior of 2D materials, we investigate the mechanics of blisters made of relatively thick 2D materials (multilayer 2D materials). We use a water-assisted wetting transfer method to prepare spontaneously formed blisters in substrate systems, including graphene/hBN, graphene/SiO$_2$, MoS$_2$/SiO$_2$, and MoS$_2$/sapphire with the thickness varying from 1.13 to 29.51 nm, 2.83 to 39.40 nm, 2.25 to 17.72 nm, and 6.85 to 15.04 nm, respectively. According to the varied profiles of blisters observed in the experiment, the transition from stretching dominated behavior to bending dominated behavior is revealed. Besides, we investigate the variable aspect ratio of blisters for cases with different layer numbers, demonstrating the breakdown of the constant aspect ratio. Furthermore, we propose an experiment-guided shape function, and further establish the theoretical model. Based on the mechanical model we present, the bending stiffness of multilayer 2D materials and the interfacial adhesion energy between 2D materials and substrates (weak or strong shear-strength interfaces) can be obtained simultaneously.
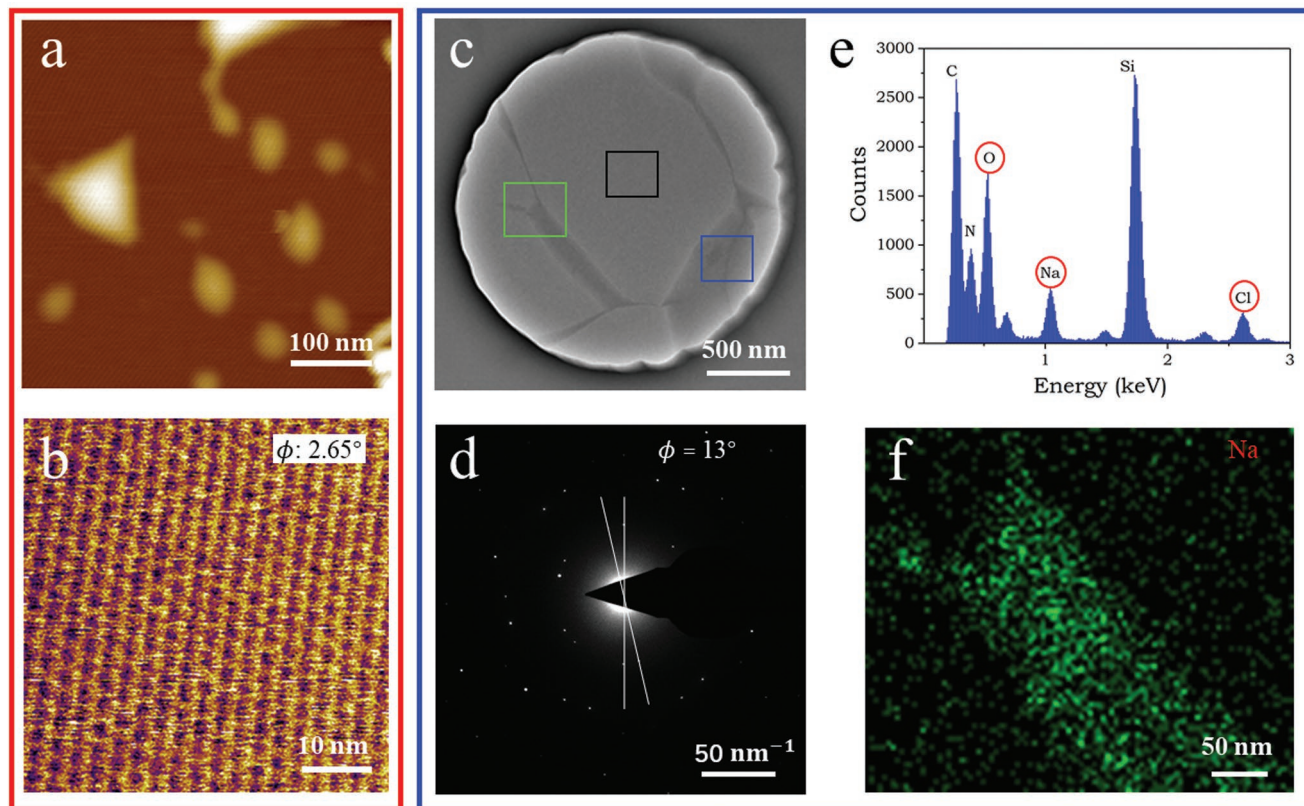
2. Results and Discussions

2.1. Blisters Formation in Graphene and MoS$_2$ Sheets

Graphene, MoS$_2$, and hBN sheets with different thicknesses are deposited onto SiO$_2$/Si or sapphire substrate via mechanical
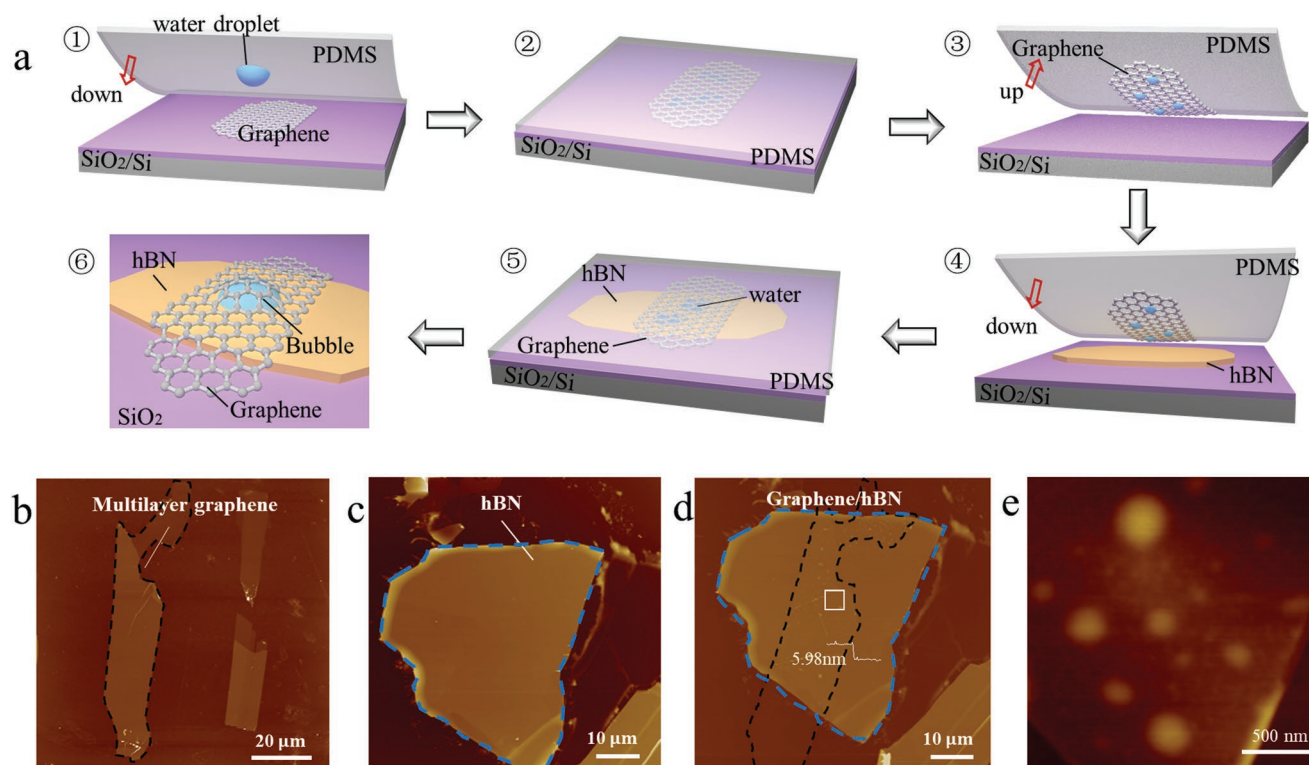
Figure 1. Preparation of water entrapped spontaneous blisters. a) Schematic diagram of water droplet-assisted transfer process. AFM images of b) multilayer graphene and hBN sheet on SiO$_2$/Si c) before and d) after transfer. e) Enlarged image of white frame region in (d). Blisters formed at the interface between multilayer graphene and hBN substrate. Dashed lines in (b)–(d) represent the outline of the graphene (black dotted line) and hBN sheets (blue dotted line), respectively.

**ADVANCED
SCIENCE NEWS**
www.advancedsciencenews.com

**ADVANCED
MATERIALS
INTERFACES**
www.advmatinterfaces.de

Figure 2. Characterization of the interface in the region of adjacent blisters and the substance inside the blisters. a) AFM image of blisters formed by monolayer graphene on an hBN substrate. b) Moiré pattern with periodic length ≈5 nm in monolayer graphene on hBN. c) TEM image of a liquid cell between graphene and hBN that is prepared using a 20 wt% NaCl aqueous solution as a transfer agent. d) Diffraction pattern taken from the black line region in (c). e,f) The results of EDX and the EDX mapping for Na element in blue and green line region in (c), respectively.

exfoliation method. According to our previous work, a water-droplet-assisted transfer method is employed to prepare spontaneously formed blisters.[35] **Figure 1**a shows the schematic drawing of the water-droplet-assisted transfer process. We use graphene as an example to discuss the transfer process. First, the droplet on the PDMS stamp is used as a lubricating agent to weaken the interfacial adhesion between the graphene sheet and SiO_2/Si substrate. Then, the graphene sheet is successfully attached to the PDMS stamp through a quick peeling force. Notably, there are water residuals on the lower surface of the graphene sheet. Finally, owing to a stronger vdW interaction between graphene and target substrate (e.g., multilayer hBN with $t > 50$ nm), the graphene sheet is successfully transferred onto an hBN substrate to form graphene/hBN heterostructure. The corresponding optical images are given in Figure S1 (Supporting Information). Note that there is no orientation control, and thus the as-fabricated heterostructures exhibit random stacking orientations between graphene and hBN. As expected, the water residuals attached to the graphene surface are intercalated between the graphene and hBN interface, forming spontaneous blisters with shape, diameter, and height heavily dependent on the graphene sheet thickness. Figure 1b–d shows the atomic force microscopy (AFM) characterization of multilayer graphene, hBN sheet before and after transfer as mentioned in Figure 1a. The enlarged AFM image in Figure 1e shows the spontaneously formed blisters with round shapes

formed by multilayer graphene ($t = 5.71$ nm, the substrate-caused offset for the bottom layer is about 0.27 nm for graphene/hBN, more information shown in Note S1, Supporting Information). To clarify the influence of interface slippage in 2D material-substrate on the blister morphology, aspect ratio, and magnitude of strain accessible within the blister region, we prepare four types of spontaneously formed blisters including graphene/hBN, graphene/SiO_2, MoS_2/SiO_2, and MoS_2/sapphire. When the substrate is SiO_2 and sapphire, respectively,[27,28,31,36–38] the interface between the 2D sheet and the substrate is often viewed as the strong-shear limit (the interface between the sheet and the substrate is fully bonded, and the edge of the blister can be viewed as the clamped boundary). In comparison, the superlubricity at graphene/hBN interface accounts for the weak-shear limit (the interface between the sheet and the substrate is ideally lubricated, and there exists slip at the edge of the blister).[39–41]

2.2. Characterization of Blisters-Free Interface and Substance inside Blisters

Earlier study revealed a thin layer of fluid coexisted with blisters, while the contamination-free interface of the rest of blister regions was demonstrated.[12] To check the atomic cleanliness of graphene/hBN interface in the blister-free regions, herein,
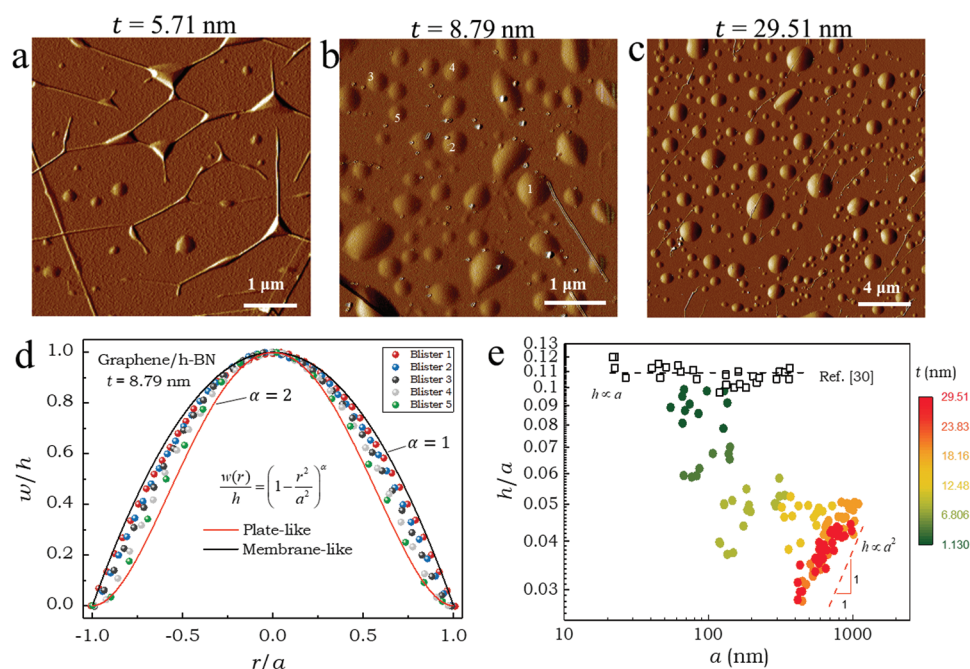
Figure 3. Morphology analysis of spontaneous blisters. a–c) AFM images of spontaneous blisters formed by graphene sheets with the thickness of 5.71, 8.79, and 29.51 nm, respectively. d) Normalized blister profiles in (b). The black and red lines correspond to a membrane-like shape with $\alpha = 1$ and a plate-like shape with $\alpha = 2$. The relevant parameters describing blister morphology include blister height h, radius a, the distance from the center r, and out-of-plane deflection $w(r)$. e) The relationship between the aspect ratio (h/a) and radius (a) with the increase of graphene layers, where black and red dashed lines correspond to membranelike and platelike, respectively. The data of black box is h/a of blisters formed by monolayer graphene on hBN.[30]

we employ friction atomic force microscopy (f-AFM) to characterize the moiré pattern of graphene/hBN heterostructures. **Figure 2**a shows that the typical AFM images of blisters of monolayer graphene/hBN heterostructure. The hexagonal-shaped moiré pattern with periodic length ≈5 nm in Figure 2b demonstrates the atomic cleanness of the interface in the region of adjacent blisters.[12,42,43] The relative rotation angle (ϕ) for graphene/hBN heterostructure can be further derived from the following form: $\lambda = \frac{(1+\delta)a}{\sqrt{2(1+\delta)(1-\cos\phi)+\delta^2}}$, where λ is the length of moiré patterns, δ is the ratio between lattice constant (0.018), a is the lattice constant of the graphene (0.246 nm).[44] Comparatively, for graphene/SiO$_2$, MoS$_2$/SiO$_2$, and MoS$_2$/sapphire systems, rather than the employment of the f-AFM technique, we assume the atomic contact in the region outside blisters. Furthermore, to demonstrate that the blisters are filled with water molecules, a liquid cell for transmission electron microscope (TEM) based on entrapment of a liquid film between graphene and hBN is prepared using a 20 wt% sodium chloride (NaCl) aqueous solution as a transfer agent instead of pure water illustrated in Figure 2c. The twist angles ($\phi = 13°$) and atomic cleanness of interface of graphene/hBN in the blister-free regions are demonstrated by two sets of hexagonal diffraction spots using selected area electron diffraction (SAED) in Figure 2d. Moreover, elemental analysis using energy dispersive X-ray (EDX) spectroscopy (Figure 2e) and the EDX mapping (Figure 2f) indicate the presence of chlorine (Cl), sodium (Na), and oxygen (O) elements inside the blisters (blue frame region in Figure 2c) and Na element evenly distributed in the blister (green frame region in Figure 2c), respectively, further

convincing the fact that the water molecules are trapped inside the blisters during the water-assisted wetting transfer process.[35]

2.3. Simultaneous Measurement of Bending Stiffness and Interfacial Adhesion Energy

The tapping mode of AFM is used to characterize the topography of the spontaneously formed blisters. **Figure 3**a–c shows the experimental observations of spontaneous blisters formed by graphene sheets on hBN substrates with different morphologies. Once increasing the thickness of the graphene layer from 5.71 to 29.51 nm, the transition from polygonal to circular blisters is observed. Specifically, for thinner graphene sheets (e.g., $t = 5.71$ nm) shown in Figure 3a, the triangular blisters with straight edges associated with visible wrinkles emanating from its vertices are common and coexist with spherical blisters. Based on the nonlinear continuum model proposed by Zhang et al.,[45] the straight-edged blisters are attributed to the development of compressive hoop strain near the periphery of the blister, triggering the nucleation of wrinkles due to the sliding of the blister boundary. However, with the increase of graphene thickness, the geometrical shapes of blisters exhibit a significant change from polygonal to quasi-circular. The dependence of blister morphology on graphene layer thickness implies the change of ability to resist out-of-plane deformation. Such variation further indicates that the bending deformation of sheets cannot be ignored for thick graphene spontaneously formed blisters.

**ADVANCED
SCIENCE NEWS**

www.advancedsciencenews.com

**ADVANCED
MATERIALS
INTERFACES**

www.advmatinterfaces.de

For simplicity, we mainly focus on approximately round-type blisters. Previous work has suggested the following function to describe the shape of a circular blister[32]

$$w(r) = h \left(1 - \frac{r^2}{a^2} \right)^{\alpha} \tag{1}$$

where $w(r)$ is the out-of-plane deflection profile, h is the blister height, a is the blister radius, and r is the distance from the blister center, $\alpha = 1$ denotes the membrane-like behavior and $\alpha = 2$ denotes the plate-like behavior. Specifically, for the pressurized blisters, the deflection profiles of blisters can be switched from plate-like (the red line in Figure 3d) to membrane-like behaviors (the black line in Figure 3d) through tuning the applied pressure difference across the membrane.[23,32] Herein, by normalizing the out-of-plane deflection of each spontaneous blister by its central height, and the radial positions by its radius, we can observe that the height profile conforms to membrane-like form for blisters formed by few-layered graphene ($t = 1.13$ or 4.41 nm) shown in Figure S3 (Supporting Information). In contrast, the collapsed deflection profiles for most of the blisters cannot be well described solely by either membrane-like or plate-like power form, but lie between these two limits (Figure 3d).

In the earlier work, the aspect ratio is demonstrated as a constant for monolayer 2D materials (e.g., graphene, hBN, MoS_2) formed spontaneous blisters on the specific substrate ($h/a \approx 0.11$ for monolayer graphene on hBN shown in the black box in Figure 3e), which is independent of the volume of the blisters.[30] Such constant aspect ratio of spontaneous blisters for a given 2D materials/substrate implied the energy competition mechanism between elastic energy and interfacial energy. Moreover, the specific aspect ratios of blisters are varied according to different types of substrates and 2D materials, showing a dependence on the elastic properties of 2D materials, interface energy as well as the surface tension of the entrapped liquid contents.[31] Generally, the contribution of bending energy in spontaneously formed blisters is ignored due to the extra-large Föppl–von Kármán number for monolayer 2D materials.[46] In our experiment, we observe that h/a keeps a constant for blisters formed by graphene sheets with few layers, but generally scatters as the layer number increases, tending to the limit of a constant h/a^2 (Figure 3e), which implies that the dome curvature, the curvature in the center of the blisters, is approximately a constant.

To quantitatively describe the variable profiles of blisters, we propose a collective shape function

$$\frac{w}{h} = \beta \left[1 - \left(\frac{r}{a} \right)^2 \right]^2 + (1 - \beta) \left[1 - \left(\frac{r}{a} \right)^2 \right] \tag{2}$$

where β, ranging from 0 to 1, is determined by fitting each blister profile with the above formula. As illustrated in **Figure 4**a, the shape of the blisters could be described well by Equation (2) with fitted β values. Figure 4b shows the distribution of geometric parameter β and the corresponding adjusted R-squared which is steadily larger than 0.95.

As stated earlier, the formation of spontaneous blisters reflects the energetic competition between the elastic energy of the deformed multilayer 2D materials and the interfacial energy associated with vdW interactions between 2D materials and substrates.[23,29–31] Based on Föppl–von Kármán equations and minimization of the total free energy, we theoretically deduce Equation (3) (see the Supporting Information for more details)

$$\Delta \gamma = \zeta E t \frac{h^4}{a^4} + D \eta \frac{h^2}{a^4} \tag{3}$$

where $\Delta \gamma$ is the energy densities (per unit area) between 2D materials and substrates, t, E, and D are the thickness, Young's modulus, and bending stiffness of 2D materials, respectively. ζ and η are functions of β and v (the Poisson's ratio of the sample) (see the Supporting Information for more details), which are illustrated in Figure 4c by taking graphene as an example with $v = 0.165$. The transformable ζ and η further indicate the necessity to introduce geometric parameter β to describe the profile of blister, instead of merely choosing a certain unified power form.

To clarify the contribution of bending stiffness of 2D materials on the profiles of blisters, we take the linear fitting equation by taking $\zeta E t \frac{h^4}{a^4}$ as the ordinate Y and $\eta \frac{h^2}{a^4}$ as the abscissa X. Given the fact that Young's modulus E of 2D materials could be easily measured with the help of nanoindentation[47] or blister testes,[32] both D and $\Delta\gamma$ could be extracted simultaneously as an
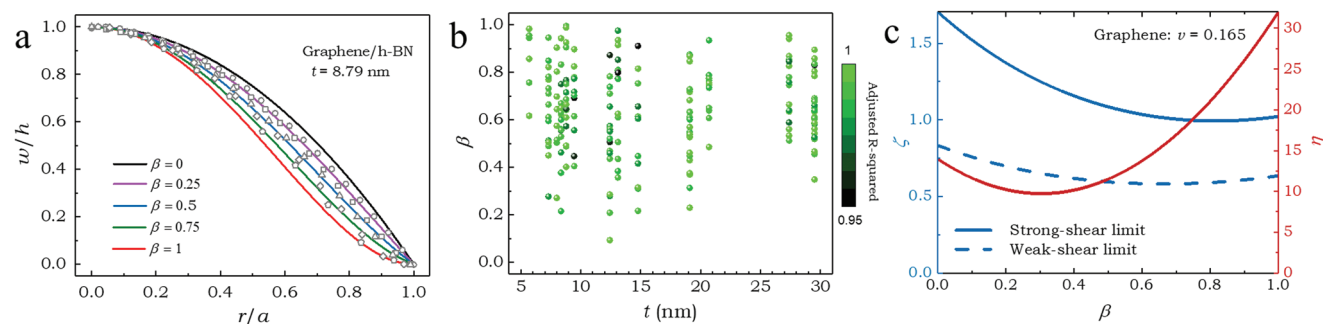
Figure 4. a) A shape function $w/h = \beta(1 - (r/a)^2)^2 + (1 - \beta)(1 - (r/a)^2)$ could describe the profile of spontaneous blisters well as β varies from 0 to 1. b) The distribution of geometric parameter β and corresponding adjusted R-squared from the AFM data fitting of multilayer graphene blisters' profiles according to Equation (2). The data are in the case of multilayer graphene on the hBN substrate. c) The dependence of ζ and η on β for two limits in case of multilayer graphene membrane with $v = 0.165$.
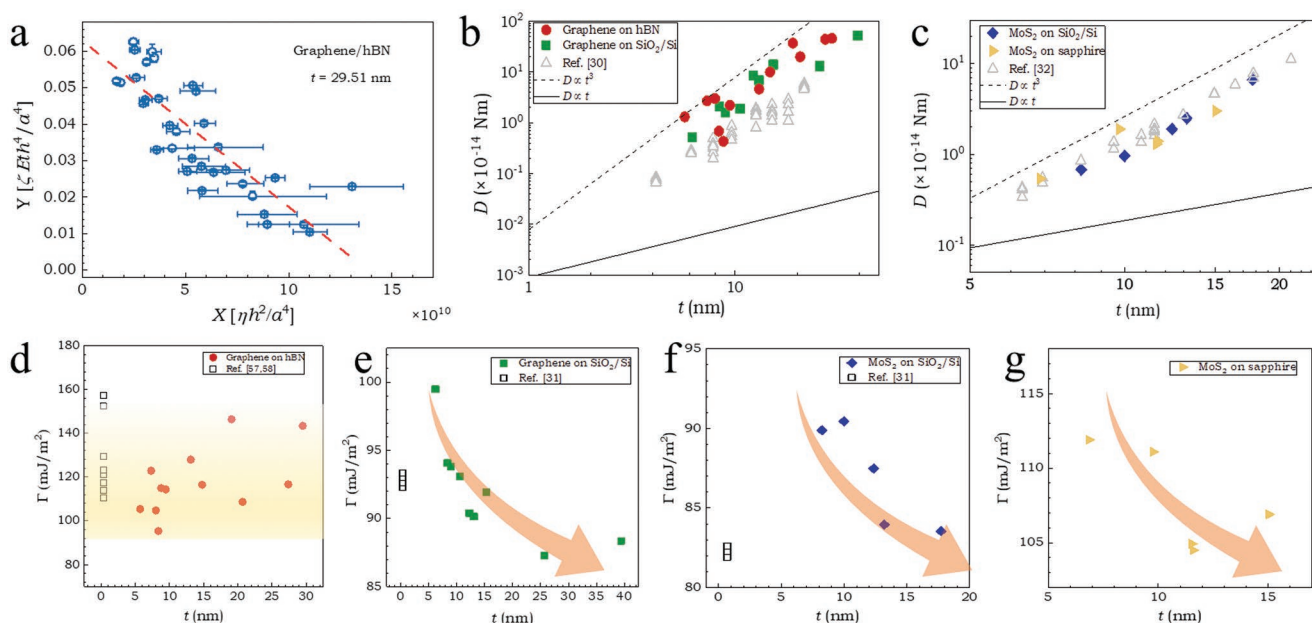
Figure 5. Bending stiffness and adhesion energy measured by spontaneous blisters. a) X, Y, and the corresponding linear fitting line obtained by analyzing 33 graphene blisters with a thickness of 29.51 nm ($N = 86$) according to Equation (3). b) Bending stiffness of multilayer graphene on an hBN sheet (red marker) and SiO_2/Si (green marker) measured by our experiments. c) Bending stiffness of multilayer MoS_2 on SiO_2/Si (blue marker) and MoS_2 on sapphire (yellow marker). The gray marker in (b) and (c) referring to the bending stiffness of graphene, MoS_2 sheets measured by gas pressurization method. d–g) The adhesion energy of interface for multilayer graphene on hBN, multilayer graphene on SiO_2/Si, multilayer MoS_2 on SiO_2/Si, and multilayer MoS_2 on sapphire, respectively. The gray marker in (d)–(f) referring to the interfacial adhesion energy of monolayer graphene, MoS_2 on hBN or SiO_2.

opposite number of the slope and the vertical intercept, respectively. Taking multilayer graphene with a thickness of 29.51 nm as an example, the derived bending stiffness and the energy densities between multilayer graphene and hBN substrate are 45×10^{-14} N m and 62.2 mJ m^{-2}, respectively, based on the data of 33 blisters (v and E as 0.165[48] and 0.939 TPa[32]). The detailed linear fitting process is shown in **Figure 5**a. Figure 5b summarizes the dependence of bending stiffness (D) for multilayer graphene sheets as a function of layer thickness. Consistent with previous expectations, the bending stiffness shows a significant growth trend as thickness increases. The specific bending stiffness at a given thickness was lower than that predicted by conventional thin plate theory in terms of $D \propto t^3$ relationship. But the results are still consistent well with our previous results based on the pressurized bulge tests,[32] where the scattered data are located within the region bounded by two theoretical limits, $D \propto t^3$ (perfectly glued interlayer interface) and $D \propto t$ (ideally lubricated interlayer interface). The observed softening of bending stiffness could be attributed to interlayer shear and sliding.[32–34,49,50] Furthermore, the derived bending stiffness of multilayer graphene sheets shows independence on the interface shear mechanics. The universality of our method is further confirmed by the results of multilayer MoS_2 blisters shown in Figure 5c.

Revisiting Equation (3), we reveal the mechanism of such mechanical response of blisters from stretching-dominated mode to bending-dominated mode as presented in Figure 3e. In detail, for the cases of graphene sheets having $t \leq 4.41$ nm, D is so small that $\zeta Et \frac{h^4}{a^4} \gg \eta D \frac{h^2}{a^4}$. Therefore, $\frac{h}{a} \cong \left(\frac{\Delta \gamma}{\zeta Et} \right)^{1/4}$ is a con-

stant independent of blister radius a. As sheet thickness further increases, it can be observed that h/a becomes highly scattered rather than a constant, implying that the effect of bending stiffness on the blister profile arises. Moreover, for the case with $t \geq 19.10$ nm, $\zeta Et \frac{h^4}{a^4} \ll \eta D \frac{h^2}{a^4}$, and h/a is gradually positively correlated with blister radius a until a new limit relationship presented, $\frac{h}{a^2} \cong \left(\frac{\Delta \gamma}{\eta D} \right)^{\frac{1}{2}}$. This phenomenon further implies that the contribution from the bending term has to be considered explicitly for the multilayer graphene spontaneously formed blisters.

It is well known that the interfacial adhesion is not only beneficial to guide the growth of 2D materials and the efficient transfer from a donor substrate to a target substrate to fabricate various 2D material based vdW devices,[35,51,52] but also a prerequisite to extract the intrinsic mechanical parameters (e.g., bending stiffness) of 2D materials through stepping methodology.[33,34] Experimentally, several methods have been developed to measure interfacial adhesion energy between 2D materials and its supported substrates, such as pressurized blister,[27,53] buckle metrology,[54] and double-cantilever beam fracture mechanics testing.[55] The interfacial adhesion energy shows dependence on the layer thickness as well as the atomic smoothness of substrates. For example, the interfacial adhesion energy for monolayer graphene on SiO_2/Si substrate was around 0.45 J m^{-2}.[27] The interfacial adhesion energy decreases with the increase of thickness for samples on SiO_2/Si substrate with great roughness,[56] indicating the non-trivial pinning effect. For a gas-filled blister,

**ADVANCED
SCIENCE NEWS**

www.advancedsciencenews.com

**ADVANCED
MATERIALS
INTERFACES**

www.advmatinterfaces.de

$\Delta\gamma$ is simply taken as the adhesion energy between 2D materials and substrate. However, for a water-filled blister, various interfaces due to the presence of water, 2D materials, and the substrate need to be considered. According to Young's equation, the adhesion energy can be obtained from[31]

$$\Gamma = \Delta\gamma + \gamma_w \left(\cos\theta_m + \cos\theta_s\right) \tag{4}$$

where Γ is the work of adhesion (or adhesion energy) of the 2D materials–target interface, γ_w is the surface tension of water (≈ 0.072 J m^{-2}), and θ_m and θ_s are the water contact angles of the 2D materials and the substrate, respectively.[31]

Interestingly, the adhesion energy Γ displays different trends for hBN, SiO$_2$/Si and sapphire substrates shown in Figure 5d–g. Surprisingly, for the graphene/hBN system, the extracted interfacial adhesion energy (95.36– 147.16 mJ m^{-2}) shows independence on the layer thickness, agreeing well with the values reported in the literature (110.1–156.2 mJ m^{-2} for graphene/hBN).[57,58] In addition, Figure 5e–g shows the apparent decreased trend of interfacial adhesion energy for graphene and MoS$_2$ sheets with the increase of layer thickness, respectively. Such a downward trend is well consistent with the earlier report,[25] and the values are in the range of 87.29– 100.50, 83.54– 90.45, and 106.9– 111.9 mJ m^{-2} for graphene/SiO$_2$, MoS$_2$/SiO$_2$, and MoS$_2$/sapphire, respectively. We attribute the discrepancy of interfacial adhesion energy to the effect of substrate roughness and interfacial interaction between substrate and transferred materials. Specifically, the surface roughness of hBN ($R_q = 0.28$ nm) is about one third of SiO$_2$/Si ($R_q = 0.86$ nm) by AFM characterization, indicating the pinning effect is indistinguishable for atomically smooth hBN substrate. Similarly, the relatively small surface roughness ($R_q = 0.37$ nm) of sapphire substrate implies that the pinning effect is negligible for MoS$_2$/sapphire system. It is worth noting, however, the derived interfacial adhesion energy between MoS$_2$/sapphire is higher than that of MoS$_2$/SiO$_2$, further indicating the strong interfacial interaction due to the dangling bond within sapphire surface. Consequently, besides the surface roughness, the interfacial interaction affects adhesion energy greatly.

3. Conclusion

In this paper, we fabricate spontaneous blisters formed by graphene and MoS$_2$ sheets using a facial water-assisted wetting transfer method. The atomic cleanliness of the interface in the blister-free regions and the blisters filled with water molecules are demonstrated by f-AFM and EDX, respectively. On the basis of an experiment-guided shape function and theoretical analysis, the effect of 2D materials thickness on the morphology of spontaneous blisters in terms of blister shapes, profiles, and aspect ratios are systematically investigated. Meanwhile, we determine the bending stiffness of multilayer 2D materials and the adhesion energy between multilayer 2D materials and substrates, simultaneously. The method is fast, easy, but robust, adding an alternative experimental way to detect unusual mechanical properties of such atomic structures.

4. Experimental Section

Materials Preparation: The wafers (285 nm SiO$_2$/Si substrates) with $\approx 1 \times 1$ cm^2 sizes were cleaned by ultrasonic in acetone, isopropyl alcohol, and deionized water for 15 min, and dried in air. Sheets of graphene, hBN, and MoS$_2$ were mechanically cleaved from the surface of their bulk by Scotch tape peeling. To prepare large-area 2D sheets, the wafers were processed by oxygen plasma (CPC-A, CIF) for 4 min and additional heat treatment. Suitable graphene and MoS$_2$ sheets were identified by a combination of optical microscopy and AFM.

Blisters Preparation: Spontaneous blisters were prepared using a water-assisted wetting transfer method in ambient air.[35] The PDMS solution was made by using a mixture of Sylgard 184 prepolymer and curing agent with a 10:1 wt% ratio and then cured at 80 °C for 2 h in a vacuum dryer. The PDMS thin film was cut into 3×3 mm pieces and attached on a glass slide due to the polarity of the group (such as Si—OH, Si—O bond, and amino group). The slide with PDMS was attached to a micromanipulator. Then, PDMS having water droplet was slightly contacted 2D materials (Figure S1c, Supporting Information) to form the structure of PDMS/2D materials/SiO$_2$. Due to the stronger wettability of water with SiO$_2$/Si, the water would infiltrate into the 2D materials and the SiO$_2$/Si substrate, thus breaking the interaction, so the 2D material can be successfully transferred to the PDMS film when the PDMS stamp was quickly peeled off by lifting the stage. It should be noticed that the PDMS must contact 2D materials first to ensure the integrity of 2D materials. In parallel, a small part of water droplets would adhere to the surface of 2D materials together to be raised. Thanks to a stronger vdW interaction between 2D materials and target substrate, 2D materials were easily transferred from PDMS to target substrate. Water droplets attached to 2D materials were trapped between them, forming spontaneous blisters.

AFM Characterization: The AFM (Asylum Research Cypher) was used to obtain atomic-resolution images and moiré pattern images (SiNi tip with resonance frequency: 10 kHz, stiffness: 0.06 N m^{-1}, and length of the cantilever: 200 μm). The AFM (Multimode 8HR, Bruker) in the standard tapping mode was used to measure the topography of the spontaneous blisters, including the height profile. RTSEP-300 silicon tip was selected as the probe with a resonance frequency of 300 kHz and stiffness of 40 N m^{-1}. And the scanning frequency was 1 Hz.

TEM Characterization: TEM images and SAED were conducted in a field emission FEI Tecnai G2 F20 microscope (FEI, USA) operated at 200 kV. The electron flux rate in the experiments ranged from 4000 to 12 000 electrons Å^{-2} s^{-1}.

Supporting Information

Supporting Information is available from the Wiley Online Library or from the author.

Conflict of Interest

The authors declare no conflict of interest.

Data Availability Statement

The data that support the findings of this study are available from the corresponding author upon reasonable request.

[1] A. Juel, D. Pihler-Puzović, M. Heil, *Annu. Rev. Fluid Mech.* **2018**, *50*, 691.

[2] D. Vella, J. Bico, A. Boudaoud, P. M. Reis, *Proc. Natl. Acad. Sci. USA* **2009**, *106*, 10901.

[3] J. Yang, X. Zhang, Y. Liu, Z. Tai, X. Yan, J. Ma, *Adv. Mater. Interfaces* **2021**, *8*, 2001899.

[4] D. A. Sanchez, Z. Dai, N. Lu, *Trends Chem.* **2021**, *14*, 00236.

[5] P. Ares, Y. B. Wang, C. R. Woods, J. Dougherty, L. Fumagalli, F. Guinea, B. Davidovitch, K. S. Novoselov, *Proc. Natl. Acad. Sci. USA* **2021**, *118*, e2025870118.

[6] L. Wang, I. Meric, P. Y. Huang, Q. Gao, Y. Gao, H. Tran, T. Taniguchi, K. Watanabe, L. M. Campos, D. A. Muller, J. Guo, P. Kim, J. Hone, K. L. Shepard, C. R. Dean, *Science* **2013**, *342*, 614.

[7] A. Jain, P. Bharadwaj, S. Heeg, M. Parzefall, T. Taniguchi, K. Watanabe, L. Novotny, *Nanotechnology* **2018**, *29*, 265203.

[8] T. Uwanno, Y. Hattori, T. Taniguchi, K. Watanable, K. Nagashio, *2D Mater.* **2015**, *2*, 041002.

[9] F. Pizzocchero, L. Gammelgaard, B. S. Jessen, J. M. Caridad, L. Wang, J. Hone, P. Boggild, T. J. Booth, *Nat. Commun.* **2016**, *7*, 11894.

[10] M. R. Rosenberger, H. J. Chuang, K. M. McCreary, A. T. Hanbicki, S. V. Sivaram, B. T. Jonker, *ACS Appl. Mater. Interfaces* **2018**, *10*, 10379.

[11] D. G. Purdie, N. M. Pugno, T. Taniguchi, K. Watanabe, A. C. Ferrari, A. Lombardo, *Nat. Commun.* **2018**, *9*, 5387.

[12] Y. Hou, Z. Dai, S. Zhang, S. Feng, G. Wang, L. Liu, Z. Xu, Q. Li, Z. Zhong, *Nat. Commun.* **2021**, *12*, 5069.

[13] V. Guerra, T. McNally, *Adv. Mater. Interfaces* **2020**, *7*, 2000944.

[14] Z. Dai, L. Liu, Z. Zhong, *Adv. Mater.* **2019**, *31*, 1805417.

[15] N. Levy, S. A. Burke, K. L. Meaker, M. Panlasigui, A. Zettl, F. Guinea, A. H. Castro Neto, M. F. Crommie, *Science* **2010**, *329*, 544.

[16] P. Ares, T. Cea, M. Holwill, Y. B. Wang, R. Roldan, F. Guinea, D. V. Andreeva, L. Fumagalli, K. S. Novoselov, C. R. Woods, *Adv. Mater.* **2020**, *32*, 1905504.

[17] Z. Fei, J. J. t. Foley, W. Gannett, M. K. Liu, S. Dai, G. X. Ni, A. Zettl, M. M. Fogler, G. P. Wiederrecht, S. K. Gray, D. N. Basov, *Nano Lett.* **2016**, *16*, 7842.

[18] D. Lloyd, X. Liu, J. W. Christopher, L. Cantley, A. Wadehra, B. L. Kim, B. B. Goldberg, A. K. Swan, J. S. Bunch, *Nano Lett.* **2016**, *16*, 5836.

[19] T. P. Darlington, C. Carmesin, M. Florian, E. Yanev, O. Ajayi, J. Ardelean, D. A. Rhodes, A. Ghiotto, A. Krayev, K. Watanabe, T. Taniguchi, J. W. Kysar, A. N. Pasupathy, J. C. Hone, F. Jahnke, N. J. Borys, P. J. Schuck, *Nat. Nanotechnol.* **2020**, *15*, 854.

[20] C. H. Lim, A. Sorkin, Q. Bao, A. Li, K. Zhang, M. Nesladek, K. P. Loh, *Nat. Commun.* **2013**, *4*, 1556.

[21] K. S. Vasu, E. Prestat, J. Abraham, J. Dix, R. J. Kashtiban, J. Beheshtian, J. Sloan, P. Carbone, M. Neek-Amal, S. J. Haigh, A. K. Geim, R. R. Nair, *Nat. Commun.* **2016**, *7*, 12168.

[22] J. M. Yuk, J. Park, P. Ercius, K. Kim, D. J. Hellebusch, M. F. Crommie, J. Y. Lee, A. Zettl, A. P. Alivisatos, *Science* **2012**, *336*, 61.

[23] K. Yue, W. Gao, R. Huang, K. M. Liechti, *J. Appl. Phys.* **2012**, *112*, 083512.

[24] P. Wang, W. Gao, Z. Cao, K. M. Liechti, R. Huang, *J. Appl. Mech.* **2013**, *80*, 040905.

[25] E. Blundo, T. Yildirim, G. Pettinari, A. Polimeni, *Phys. Rev. Lett.* **2021**, *127*, 046101.

[26] N. G. Boddeti, S. P. Koenig, R. Long, J. Xiao, J. S. Bunch, M. L. Dunn, *J. Appl. Mech.* **2013**, *80*, 040909.

[27] S. P. Koenig, N. G. Boddeti, M. L. Dunn, J. S. Bunch, *Nat. Nanotechnol.* **2011**, *6*, 543.

[28] G. Wang, Z. Dai, Y. Wang, P. Tan, L. Liu, Z. Xu, Y. Wei, R. Huang, Z. Zhang, *Phys. Rev. Lett.* **2017**, *119*, 036101.

[29] Z. Dai, Y. Hou, D. A. Sanchez, G. Wang, C. J. Brennan, Z. Zhang, L. Liu, N. Lu, *Phys. Rev. Lett.* **2018**, *121*, 266101.

[30] E. Khestanova, F. Guinea, L. Fumagalli, A. K. Geim, I. V. Grigorieva, *Nat. Commun.* **2016**, *7*, 12587.

[31] D. A. Sanchez, Z. Dai, P. Wang, A. Cantu-Chavez, C. J. Brennan, R. Huang, N. Lu, *Proc. Natl. Acad. Sci. USA* **2018**, *115*, 7884.

[32] G. Wang, Z. Dai, J. Xiao, S. Feng, C. Weng, L. Liu, Z. Xu, R. Huang, Z. Zhang, *Phys. Rev. Lett.* **2019**, *123*, 116101.

[33] E. Han, J. Yu, E. Annevelink, J. Son, D. A. Kang, K. Watanabe, T. Taniguchi, E. Ertekin, P. Y. Huang, A. M. van der Zande, *Nat. Mater.* **2020**, *19*, 305.

[34] J. Yu, E. Han, M. A. Hossain, K. Watanabe, T. Taniguchi, E. Ertekin, A. M. van der Zande, P. Y. Huang, *Adv. Mater.* **2021**, *33*, 2007269.

[35] Y. Hou, X. Ren, J. Fan, G. Wang, Z. Dai, C. Jin, W. Wang, Y. Zhu, S. Zhang, L. Liu, Z. Zhang, *ACS Appl. Mater. Interfaces* **2020**, *12*, 40958.

[36] Z. Dou, Z. Chen, N. Li, S. Yang, Z. Yu, Y. Sun, Y. Li, B. Liu, Q. Luo, T. Ma, L. Liao, Z. Liu, P. Gao, *Nat. Commun.* **2019**, *10*, 5013.

[37] N. Nayir, Y. K. Shin, Y. Wang, M. Y. Sengul, D. R. Hickey, M. Chubarov, T. H. Choudhury, N. Alem, J. Redwing, V. H. Crespi, A. C. T. van Duin, *J. Phys. Chem. C* **2021**, *125*, 17950.

[38] T. Li, W. Guo, L. Ma, W. Li, Z. Yu, Z. Han, S. Gao, L. Liu, D. Fan, Z. Wang, Y. Yang, W. Lin, Z. Luo, X. Chen, N. Dai, X. Tu, D. Pan, Y. Yao, P. Wang, Y. Nie, J. Wang, Y. Shi, X. Wang, *Nat. Nanotechnol.* **2021**, *16*, 1201

[39] Y. Song, D. Mandelli, O. Hod, M. Urbakh, M. Ma, Q. Zheng, *Nat. Mater.* **2018**, *17*, 894.

[40] D. Mandelli, I. Leven, O. Hod, M. Urbakh, *Sci. Rep.* **2017**, *7*, 10851.

[41] I. Leven, D. Krepel, O. Shemesh, O. Hod, *J. Phys. Chem. Lett.* **2013**, *4*, 115.

[42] J. Xue, J. Sanchez-Yamagishi, D. Bulmash, P. Jacquod, A. Deshpande, K. Watanabe, T. Taniguchi, P. Jarillo-Herrero, B. J. LeRoy, *Nat. Mater.* **2011**, *10*, 282.

[43] R. Decker, Y. Wang, V. W. Brar, W. Regan, H. Z. Tsai, Q. Wu, W. Gannett, A. Zettl, M. F. Crommie, *Nano Lett.* **2011**, *11*, 2291.

[44] M. Yankowitz, Q. Ma, P. Jarillo-Herrero, B. J. LeRoy, *Nat. Rev. Phys.* **2019**, *1*, 112.

[45] K. Zhang, M. Arroyo, *Extreme Mech. Lett.* **2017**, *14*, 23.

[46] M. K. Blees, A. W. Barnard, P. A. Rose, S. P. Roberts, K. L. McGill, P. Y. Huang, A. R. Ruyack, J. W. Kevek, B. Kobrin, D. A. Muller, P. L. McEuen, *Nature* **2015**, *524*, 204.

[47] C. Lee, X. Wei, J. W. Kysar, J. Hone, *Science* **2008**, *321*, 385.

[48] H. Li, A. W. Contryman, X. Qian, S. M. Ardakani, Y. Gong, X. Wang, J. M. Weisse, C. H. Lee, J. Zhao, P. M. Ajayan, J. Li, H. C. Manoharan, X. Zheng, *Nat. Commun.* **2015**, *6*, 7381.

[49] X. Ma, L. Liu, Z. Zhong, Y. Wei, *J. Appl. Mech.* **2021**, *88*, 011004.

[50] F. Pan, G. Wang, L. Liu, Y. Chen, Z. Zhong, X. Shi, *J. Mech. Phys. Solids* **2019**, *122*, 340.

[51] M. Mattinen, P. J. King, P. Brüner, M. Leskel, M. Ritala, *Adv. Mater. Interfaces* **2020**, *7*, 2001046.

[52] J. Zhou, H. Chen, X. Zhang, K. Chi, Y. Cai, Y.. Cao, J. Pang, *J. Alloys Compd.* **2021**, *862*, 158703.

[53] C. D. Giorgio, E. Blundo, G. Pettinari, M. Felici, Y. Lu, A. M. Cucolo, A. Polimeni, F. Bobba, *Adv. Mater. Interfaces* **2020**, *7*, 2001024.

[54] C. J. Brennan, J. Nguyen, E. T. Yu, N. Lu, *Adv. Mater. Interfaces* **2015**, *2*, 1500176.

[55] T. Yoon, W. C. Shin, T. Y. Kim, J. H. Mun, T. S. Kim, B. J. Cho, *Nano Lett.* **2012**, *12*, 1448.

[56] C. R. Dean, A. F. Young, I. Meric, C. Lee, L. Wang, S. Sorgenfrei, K. Watanabe, T. Taniguchi, P. Kim, K. L. Shepard, J. Hone, *Nat. Nanotechnol.* **2010**, *5*, 722.

[57] S. J. Haigh, A. Gholinia, R. Jalil, S. Romani, L. Britnell, D. C. Elias, K. S. Novoselov, L. A. Ponomarenko, A. K. Geim, R. Gorbachev, *Nat. Mater.* **2012**, *11*, 764.

[58] S. R. Na, J. W. Suk, R. S. Ruoff, R. Huang, K. M. Liechti, *ACS Nano* **2014**, *8*, 11234.